

SplitLoRA: Balancing Stability and Plasticity in Continual Learning Through Gradient Space Splitting

Haomiao Qiu^{1,2}, Miao Zhang^{1*}, Ziyue Qiao^{2*}, Weili Guan¹, Min Zhang¹, Liqiang Nie¹

¹ Harbin Institute of Technology (Shenzhen)

² Great Bay University

24B951058@stu.hit.edu.cn, zhangmiao@hit.edu.cn, zyqiao@gbu.edu.cn
honeyguan@gmail.com, zhangmin2021@hit.edu.cn, nieliqiang@gmail.com

Abstract

Continual Learning (CL) requires a model to learn multiple tasks in sequence while maintaining both stability—preserving knowledge from previously learned tasks, and plasticity—effectively learning new tasks. Gradient projection has emerged as an effective and popular paradigm in CL, where it partitions the gradient space of previously learned tasks into two orthogonal subspaces: a primary subspace and a minor subspace. New tasks are learned effectively within the minor subspace, thereby reducing interference with previously acquired knowledge. However, existing Gradient Projection methods struggle to achieve an optimal balance between plasticity and stability, as it is hard to appropriately partition the gradient space. In this work, we consider a continual learning paradigm based on Low-Rank Adaptation (LoRA), which has gained considerable attention due to its efficiency and wide applicability, and propose a novel approach for continual learning, called SplitLoRA. We first provide a theoretical analysis of how subspace partitioning affects model stability and plasticity. Informed by this analysis, we then introduce an effective method that derives the optimal partition of the gradient space for previously learned tasks. This approach effectively balances stability and plasticity in continual learning. Experimental results on multiple datasets demonstrate that the proposed method achieves state-of-the-art performance.

1 Introduction

Continual Learning (CL) refers to a model’s ability to sequentially learn new tasks while retaining knowledge from previously learned tasks [1]. This contrasts with traditional machine learning paradigms, which assume that models are trained on a fixed dataset where all data is available at once. In the CL setting, the challenge lies in maintaining performance on previous tasks while adapting to new ones, necessitating a balance between stability and plasticity. In recent years, orthogonal projection methods have demonstrated strong performance in continual learning tasks. These methods require storing the subspace spanned by the gradients of previous tasks in memory. During new task training, the gradient of the current task is projected onto the minor subspace of the previous task’s gradient subspace, reducing the interference of new task updates with previously learned knowledge.

Parameter-Efficient Fine-Tuning (PEFT) [2, 3, 4] enables efficient fine-tuning for new tasks by keeping the pre-trained model parameters unchanged while introducing a small subset of trainable parameters. Due to its advantages in computational efficiency and performance, PEFT methods have gained increasing popularity in continual learning [5, 6, 7, 8, 9]. Combining orthogonal projection with PEFT can better leverage the knowledge of the pre-trained model, allowing for faster adaptation to new tasks.

*Co-corresponding Authors.

However, existing methods [8, 9] typically determine the subspace dimension for each module within the model by using a predefined threshold based on the cumulative sum of squared singular values. This approach enforces a uniform partitioning rule across all modules, ignoring the fact that different modules contribute unequally to knowledge retention [10, 11, 12]. As a result, it fails to achieve an optimal trade-off between stability and plasticity.

In this paper, we theoretically analyze the relationship between the size of the minor gradient subspace of previous tasks and the upper bound of loss increments across all tasks. Furthermore, we model its impact on both stability and plasticity. In practice, we build upon the LoRA framework and propose a novel method called SplitLoRA for CL tasks. Specifically, to minimize the upper bound of the total task loss growth, we construct an optimization problem to determine the optimal size of minor subspace and derive an approximate solution to balance stability and plasticity.

Our contributions are summarized as follows:

- We theoretically model the impact of the gradient subspace size of previous tasks on stability and plasticity in orthogonal projection based continual learning in Theorem 4.2 and derive an approximate optimal minor subspace in CL.
- We introduce SplitLoRA, a novel PEFT framework. By projecting the minor subspace onto the LoRA dimension reduction matrix \mathbf{A}_t via a random projection and optimizing only \mathbf{B}_t , SplitLoRA ensures that updates remain confined to the minor subspace, thereby achieving an effective balance between stability and plasticity.
- Our method achieves state-of-the-art performance across multiple datasets, surpassing existing CL methods by 2%–5% on different datasets.

2 Related Work

2.1 Parameter-Efficient Fine-Tuning

Parameter-efficient fine-tuning modifies pre-trained models by introducing a small set of trainable parameters while keeping the original model frozen, significantly reducing computational costs while maintaining strong performance. Adapter [3] fine-tunes small modules added to multiple layers, while Prompt-tuning [13] and Prefix-tuning [14] inject trainable tokens into Transformer layers. LoRA [2] decomposes weight updates into low-rank matrices, tuning only these structures. Despite training fewer parameters, PEFT methods often achieve comparable or superior performance [15, 16, 2, 17]. Initially developed for NLP, PEFT has been extended to vision tasks, with methods such as Visual Prompt Tuning (VPT) [4] and AdapterFormer [18] achieving performance on par with full fine-tuning.

2.2 Continual Learning

Continual learning methods fall into three main categories: regularization-based, memory-based, and expansion-based. Regularization-based approaches [19, 20, 21, 22] constrain significant changes to key parameters to mitigate catastrophic forgetting. Memory-based methods [23, 24, 25, 26] retain prior task information in a buffer, allowing models to revisit past knowledge. Expansion-based techniques [27, 28, 29] dynamically expand the model architecture to accommodate new tasks while preserving learned representations.

Gradient Projection in CL. Gradient projection [30, 31, 32] mitigates task interference by constraining updates to directions orthogonal to previous tasks. Orthogonal Weight Modulation [30] learns a projector matrix to prevent new gradients from overwriting prior knowledge. Orthogonal Gradient Descent [31] projects new gradients onto the orthogonal complement of previous task gradients. Gradient Projection Memory (GPM) [32] stores subspace bases of old task data and projects new gradients onto their orthogonal complement. Trust Region Gradient [33] enhances forward knowledge transfer by leveraging task-related representations.

PEFT in CL. With the rise of pre-trained models [34, 35, 36], continual learning has shifted toward leveraging them rather than training from scratch. While some approaches [37, 38] fine-tune pre-trained models fully, this is often inefficient. To address this, PEFT methods have been explored in continual learning, with studies [6, 5, 39, 40] integrating prompt-tuning to improve class-incremental

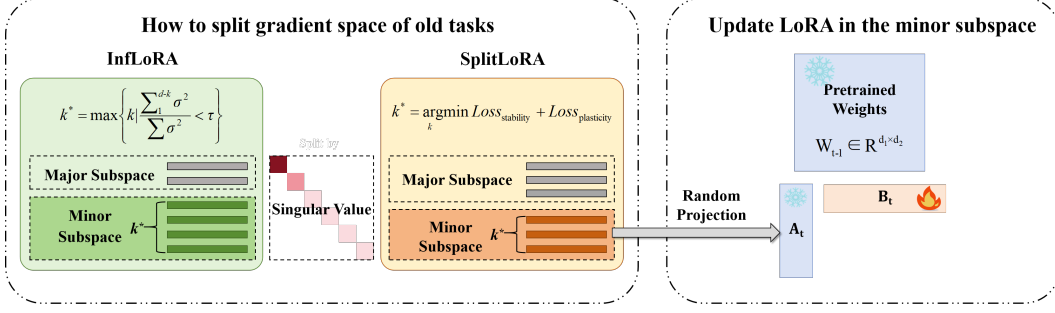


Figure 1: An overview of our proposed SplitLoRA. During the learning of the t -th task, the gradient space of tasks 1 to $t - 1$ is decomposed into major and minor subspaces. InfLoRA determines k^* solely based on a predefined threshold, whereas SplitLoRA balances stability loss and plasticity loss to determine k^* . Then the minor subspaces are randomly projected onto the low-dimensional matrix A of LoRA and fixed, while only B is trained. Specifically, $W_{t-1} = W_0 + \sum_{i=1}^{t-1} A_i B_i$, where W_0 represents the pre-trained model weights, and k denotes the size of the minor subspace.

learning. A unified framework [7] further combines various PEFT techniques, including prompt-tuning, LoRA, and Adapter, into continual learning.

3 Preliminary

3.1 Continual Learning Formulation

In CL, there are T tasks $\mathcal{T}_1, \dots, \mathcal{T}_T$, each task includes data: $\mathcal{D}_t = \{(\mathbf{x}_i^t, y_i^t)\}_{i=1}^{n_t}$, where $\mathbf{x}_i^t \in \mathbb{R}^d$ is the input and $y_i^t \in \mathbb{R}$ is the label. The goal of CL is to achieve an overall optimal performance across all tasks. Let \mathbf{W}_T represent the model parameters after training on the last task T . The loss on task t , denoted as $\mathcal{L}_t(\mathbf{W}_T)$, measures the performance of \mathbf{W}_T on task t . Let \mathbf{W}_T^* represent the optimal parameters. Then, the objective is to minimize the total loss across all tasks:

$$\mathbf{W}_T^* = \underset{\mathbf{W}_T}{\operatorname{argmin}} \mathcal{L}_{all}(\mathbf{W}_T) = \underset{\mathbf{W}_T}{\operatorname{argmin}} \sum_{t=1}^T \mathcal{L}_t(\mathbf{W}_T). \quad (1)$$

3.2 LoRA-based Continual Learning

LoRA [2] is a low-rank based PEFT method that reduces the number of parameters by decomposing the weight matrix into the product of two low-rank matrices. Specifically, for a linear layer, the extra weight matrix $\Delta \mathbf{W}$ is decomposed into two low-rank matrices \mathbf{A} and \mathbf{B} as: $\Delta \mathbf{W} = \mathbf{A}\mathbf{B}$, where $\mathbf{A} \in \mathbb{R}^{d_1 \times r}$ and $\mathbf{B} \in \mathbb{R}^{r \times d_2}$, and r is the dimension of the low-rank. In this way, the number of parameters of the weight matrix is reduced from $d_1 d_2$ to $2dr$. During training, we learn \mathbf{A} and \mathbf{B} by minimizing the loss function of the current task. During testing, we recover $\mathbf{W} = \mathbf{W}_0 + \mathbf{A}\mathbf{B}$ and use it for forward propagation.

CL generally initializes an additional LoRA for the new task t , while the LoRA of old tasks also participates in the forward process [8, 41]. In the current task t , the forward process of the linear layer is

$$\mathbf{Y} = \mathbf{W}_t \mathbf{X} = (\mathbf{W}_{t-1} + \mathbf{A}_t \mathbf{B}_t) \mathbf{X}, \quad (2)$$

and only \mathbf{A}_t and \mathbf{B}_t are trained during training.

4 SplitLoRA

In this section, we introduce SplitLoRA, a PEFT method for CL that mitigates catastrophic forgetting by partitioning the gradient space. Unlike existing Gradient Projection-based methods [8, 9, 42], which typically define the minor subspace solely based on the sum of squared singular values

being below a predefined threshold, SplitLoRA determines the optimal subspace size by analyzing the impact of the minor subspace on stability loss and plasticity loss. We first introduce gradient projection, then model the effect of subspace partitioning on learning dynamics and formulate an optimization problem to derive the approximate optimal size of the minor subspace. Finally, we present how to construct the low-rank projection matrix within this subspace to enhance CL. The entire process of SplitLoRA is illustrated in Figure 1.

4.1 Orthogonal Decomposition based Gradient Projection

Empirically, training on new tasks often leads to performance degradation on previously learned tasks due to interference between the gradients of new and old tasks, resulting in stability loss. To address this issue, GPM [32] orthogonally decomposes the gradient space of previous tasks into a major subspace and a minor subspace, and constrains the update direction of the new task within the minor subspace. Our work is also built upon orthogonal decomposition.

In CL, we aim to maintain an average gradient space \mathbf{G}^{old} for all previous tasks. Specifically, after training the task $t - 1$, we re-feed the data from this task into the model and calculate the average gradient $\mathbf{G}_{t-1}^{\text{new}}$ of W throughout this process. Finally, we compute the average gradient space $\mathbf{G}_t^{\text{old}}$ for the previous $t - 1$ tasks:

$$\mathbf{G}_t^{\text{old}} = \frac{1}{t-1}((t-2)\mathbf{G}_{t-1}^{\text{old}} + \mathbf{G}_{t-1}^{\text{new}}). \quad (3)$$

For the first task, $\mathbf{G}_1^{\text{old}}$ is equal to zero. Next, we receive the data from task t . We perform a Singular Value Decomposition (SVD) on the gradient $\mathbf{G}_t^{\text{old}}$. Larger singular values correspond to singular vectors that dominate in describing the vector’s importance. We select the last k left singular vectors of $\hat{\mathbf{U}}_t$ as the minor subspace:

$$\hat{\mathbf{U}}_t, \hat{\Sigma}_t, \hat{\mathbf{V}}_t^\top = \text{SVD}(\mathbf{G}_t^{\text{old}}), \quad \hat{\mathbf{U}}_t^k = \hat{\mathbf{U}}_t[:, -k:]. \quad (4)$$

The gradient of previous tasks has a much smaller component in the minor subspace compared to the major subspace. Therefore, projecting the gradient of the new task onto the minor subspace will result in minimal interference.

A common projection method is to construct a projection transformation matrix. For simplicity, we consider a linear layer \mathbf{W} in a model. As the model update $\Delta\mathbf{W}$ is determined by the gradient, projecting the model update onto the minor subspace is equivalent to constraining the gradient direction, which helps mitigate interference. Specifically, we project the model update $\Delta\mathbf{W}$ onto the minor subspace. The projection result is given by:

$$\Delta\hat{\mathbf{W}} = \text{proj}_{\text{col}(\hat{\mathbf{U}}_t^k)}(\Delta\mathbf{W}) = \hat{\mathbf{U}}_t^k \hat{\mathbf{U}}_t^{k\top} \Delta\mathbf{W}, \quad (5)$$

where $\hat{\mathbf{U}}_t^k$ is the projection subspace. Since the gradients of previous tasks are distributed primarily in the major subspace, therefore the projection ensures that the updates primarily benefit the new task while minimally affecting the performance of old tasks.

4.2 Minor Space Setting for Old Tasks

Projecting the gradient onto the minor subspace can mitigate interference with previous tasks. And the larger the minor subspace size k , the larger the learning space for the new task, leading to better plasticity. However, as the gradient components of previous tasks in the minor subspace increase, stability deteriorates.

Previous methods [42, 33, 8, 9] compute the sum of the squared singular values corresponding to the minor subspace, ensuring that it remains below a predefined threshold τ . Among all values of k that satisfy this condition, they select the largest one:

$$k^* = \max \left\{ k \mid \frac{\sum_{i=1}^{d-k} \sigma_i^2}{\sum \sigma_i^2} < \tau \right\}. \quad (6)$$

The size of the minor subspace, denoted as k , is a crucial parameter that affects both model stability and plasticity. However, previous methods determine k based on a predefined threshold τ , which is merely a hyperparameter and does not effectively balance stability and plasticity. Thus, we proceed to analyze how subspace selection impacts the loss across all tasks. Based on the smoothness of the loss function \mathcal{L} , we can derive an upper bound on the loss incurred due to parameter updates in CL.

Proposition 4.1 (Upper Bound on Loss Increase). *Consider a model with a linear layer updated from \mathbf{W}_{t-1} to $\mathbf{W}_t = \mathbf{W}_{t-1} + \Delta \mathbf{W}_t$. Assume the loss function is L -smooth and that the first $t-1$ tasks were trained with updates constrained to be orthogonal to the gradients of previous tasks. Then, the total loss change over tasks $1, \dots, t$ is bounded by:*

$$\sum_{i=1}^t (\mathcal{L}_i(\mathbf{W}_t) - \mathcal{L}_i(\mathbf{W}_{t-1})) \leq \underbrace{-(t-1) \langle \Delta \mathbf{W}_t, \mathbf{G}_t^{\text{old}} \rangle}_{\text{Stability Loss}} - \underbrace{\langle \Delta \mathbf{W}_t, \mathbf{G}_t \rangle}_{\text{Plasticity Loss}} + \frac{(t-1)L}{2} \|\Delta \mathbf{W}_t\|_F^2, \quad (7)$$

where $\mathbf{G}_t = \nabla \mathcal{L}_t(\mathbf{W}_t)$ is the gradient for task t , and $\mathbf{G}_t^{\text{old}} = \frac{1}{t-1} \sum_{i=1}^{t-1} \mathbf{G}_i$ is the average gradient of previous tasks. $\langle \cdot, \cdot \rangle$ denotes the Frobenius inner product.

This result shows that parameter updates affect both the current and past tasks. The term $\langle \Delta \mathbf{W}_t, \mathbf{G}_t^{\text{old}} \rangle$ captures interference with past tasks (stability loss), while $\langle \Delta \mathbf{W}_t, \mathbf{G}_t \rangle$ reflects progress on the current task (plasticity gain). The squared norm $\|\Delta \mathbf{W}_t\|_F^2$ acts as a regularization term controlled by the smoothness constant L .

Next, we discuss how to choose the minor subspace in gradient projection to minimize the combined stability and plasticity losses. Building on Proposition 1, we can theoretically analyze how stability loss and plasticity loss vary as a function of k . From Eq. (7), after replacing $\Delta \mathbf{W}_t$ with $\Delta \hat{\mathbf{W}}_t$, where $\Delta \hat{\mathbf{W}}_t = \mathbf{U}_t^k \mathbf{U}_t^{k\top} \Delta \mathbf{W}_t$ is the projected update onto the minor subspace, we can express the stability loss $\mathcal{L}_t^S(\mathbf{W}_t)$ and the plasticity loss $\mathcal{L}_t^P(\mathbf{W}_t)$ as follows:

$$\mathcal{L}_t^S(\mathbf{W}_t) = -(t-1) \langle \Delta \hat{\mathbf{W}}_t, \mathbf{G}_t^{\text{old}} \rangle, \quad (8)$$

$$\mathcal{L}_t^P(\mathbf{W}_t) = -\langle \Delta \hat{\mathbf{W}}_t, \mathbf{G}_t \rangle. \quad (9)$$

The stability loss is proportional to the alignment between the projected update $\Delta \hat{\mathbf{W}}_t$ and the gradient of old tasks $\mathbf{G}_t^{\text{old}}$, while the plasticity loss depends on the alignment of $\Delta \hat{\mathbf{W}}_t$ with the gradient of the new task \mathbf{G}_t . Then we define the error function $\epsilon(k)$, which quantifies the proportion of these minor directions and is given by:

$$\epsilon(k) = \frac{\sum_{i=d-k+1}^d \sigma_i}{\sum_{i=1}^d \sigma_i}. \quad (10)$$

$\epsilon(k)$ measures the interference error caused by updating the model within the minor subspace on old tasks. Based on Proposition 4.1, we can derive the following theorem:

Theorem 4.2. *Let \mathbf{W}_{t-1} denote the weight matrix of a linear layer in the model, updated as $\mathbf{W}_t = \mathbf{W}_{t-1} + \Delta \hat{\mathbf{W}}_t = \mathbf{W}_{t-1} + \mathbf{U}_t^k \mathbf{U}_t^{k\top} \Delta \mathbf{W}_t$. Since the update direction of the new task is unknown, we assume that it is uniformly distributed across all directions. that is to say, $\Delta \mathbf{W}_t$ has the same expected projection value across different feature directions of \mathbf{G}_t , we provide the expected values of the stability loss :*

$$\mathbb{E}[\mathcal{L}_t^S(\mathbf{W}_t)] = -(t-1)\epsilon_t(k_t) \langle \Delta \mathbf{W}_t, \mathbf{G}_t^{\text{old}} \rangle, \quad (11)$$

and the plasticity loss:

$$\mathbb{E}[\mathcal{L}_t^P(\mathbf{W}_t)] = -\frac{k_t}{d} \langle \Delta \mathbf{W}_t, \mathbf{G}_t \rangle. \quad (12)$$

The proof of this theorem can be found in Appendix A.2. Therefore, achieving an optimal balance between these two objectives requires solving the following optimization problem:

$$k_t^* = \underset{k}{\operatorname{argmin}} (\mathbb{E}[\mathcal{L}_t^F(\mathbf{W}_t)] + \mathbb{E}[\mathcal{L}_t^P(\mathbf{W}_t)]). \quad (13)$$

Noting that $\Delta \mathbf{W}_t$ and \mathbf{G}_t gradually change as training progresses, solving this optimization problem is challenging. To simplify this, we introduce a ratio parameter α :

$$\alpha = -\frac{\langle \Delta \mathbf{W}_t, \mathbf{G}_t \rangle}{\langle \Delta \mathbf{W}_t, \mathbf{G}_t^{\text{old}} \rangle}. \quad (14)$$

Algorithm 1 SplitLoRA

```
1: Input: Datasets  $\mathcal{D}_t = \{(\mathbf{x}_i^t, y_i^t)\}_{i=1}^{n_t}$ , for  $T$  tasks  $\mathcal{T}_1, \dots, \mathcal{T}_T$ , a pre-trained ViT model  $f_{\Theta}(\cdot)$  with  $l$  layers.  
2: Output: The optimized  $\mathbf{W}_T^l$  for each layer  $l$ .  
3: Initialization:  $\mathbf{G}_1^{\text{old}} = \mathbf{0}$   
4: for  $t = 1$  to  $T$  do  
5:   if  $t > 1$  then  
6:     Compute  $k_t$  using Eq. (15) for each LoRA module  
7:     Initialize  $\mathbf{A}_t$  using Eq. (17) for each LoRA module  
8:   end if  
9:   Train LoRA on task  $\mathcal{T}_t$  using dataset  $\mathcal{D}_t$   
10:  Update  $\mathbf{G}_t^{\text{old}}$  using Eq. (3) for each layer  
11: end for
```

This substitution reformulates the optimization problem into the following form:

$$k_t^* = \underset{k}{\operatorname{argmin}} \left((t-1)\epsilon_t(k_t) - \alpha \frac{k_t}{d} \right). \quad (15)$$

Since $\Delta \mathbf{W}_t$ benefits new tasks, it often interferes with previous task knowledge, leading to:

$$\langle \Delta \mathbf{W}_t, \mathbf{G}_t \rangle > 0, \quad \langle \Delta \mathbf{W}_t, \hat{\mathbf{G}}_t \rangle < 0. \quad (16)$$

From Eq. (15), it is evident that increasing k_t leads to higher $\epsilon_t(k_t)$, which increases stability loss \mathcal{L}_t^F , while expanding the learning space and thus reducing plasticity loss \mathcal{L}_t^P . However, since both $\Delta \mathbf{W}_t$ and \mathbf{G}_t change during training, α also varies dynamically. Meanwhile, the update subspace must be determined before training begins for task t . To resolve this mismatch, we treat α as a fixed hyperparameter throughout the learning process. In our experiments, α was set as a hyperparameter, with $\alpha = 20$ as a general choice. Further experimental analysis indicates that our method is highly robust to α in Table 4.

In the simplified optimization problem of Eq.(15), the parameter k_t is restricted to integer values within the range $[1, d]$. The optimal solution to this equation can be obtained by evaluating the objective function for all possible values of k_t and selecting the one that minimizes it as k_t^* . For example, in ViT-B/16 [35], embedding dimension is 768, and k can be selected as any integer between 1 and 768. It is worth noting that we compute k separately for each LoRA module, as weights at different layers and positions capture substantially different knowledge. A fixed threshold, as used in InfLoRA [8], cannot effectively account for such variation across modules.

4.3 LoRA Updates in the Minor Subspace

To ensure LoRA updates remain within the minor subspace, we fix the projection matrix \mathbf{A}_t and only optimize \mathbf{B}_t . LoRA parameterizes the weight update as: $\Delta \mathbf{W}_t = \mathbf{A}_t \mathbf{B}_t$. When \mathbf{A}_t is fixed, the update is confined to its column space [8, 41]. To restrict this space to the minor subspace of previous tasks, we construct

$$\mathbf{A}_t = \hat{\mathbf{U}}_t^k \mathbf{R}, \quad (17)$$

where $\hat{\mathbf{U}}_t^k \in \mathbb{R}^{d \times k}$ is an orthonormal basis of the minor subspace and $\mathbf{R} \in \mathbb{R}^{k \times r}$ is a random Gaussian matrix. Importantly, this constraint only holds if \mathbf{A}_t remains fixed during training, otherwise, the update direction may drift out of the subspace. Fortunately, prior works [43, 8] verify that fixing \mathbf{A}_t maintains sufficient model capacity while controlling interference. This design ensures that task updates are constrained to low-interference directions $\hat{\mathbf{U}}_t^k$, balancing stability and plasticity without additional memory or computational cost. The full procedure of SplitLoRA is summarized in Algorithm 1.

Table 1: We present FAA (%) and CAA(%) on ImageNet-R under three incremental learning settings: “5-task,” “10-task,” and “20-task.” All backbone networks are pre-trained on ImageNet-21K.

Method	Pub.	5-task		10-task		20-task	
		FAA (↑)	CAA (↑)	FAA (↑)	CAA (↑)	FAA (↑)	CAA (↑)
Upper-bound	—	84.09 ± 0.21	—	84.09 ± 0.21	—	84.09 ± 0.21	—
FT	—	18.74 ± 0.44	48.39 ± 0.58	10.12 ± 0.51	35.23 ± 0.92	4.75 ± 0.40	22.8 ± 0.37
FT++	—	60.42 ± 0.87	71.59 ± 0.50	48.93 ± 1.15	66.79 ± 0.92	35.98 ± 1.38	59.68 ± 0.95
L2P++ [5]	CVPR22	70.83 ± 0.58	78.34 ± 0.47	69.29 ± 0.73	78.30 ± 0.69	65.89 ± 1.30	77.15 ± 0.65
Deep L2P++ [5]	CVPR22	73.93 ± 0.37	80.14 ± 0.54	71.66 ± 0.64	79.63 ± 0.90	68.42 ± 1.20	78.68 ± 1.03
DualPrompt [44]	ECCV22	73.05 ± 0.50	79.47 ± 0.40	71.32 ± 0.62	78.94 ± 0.72	67.87 ± 1.39	77.42 ± 0.80
CODA-P [6]	CVPR23	76.51 ± 0.38	82.04 ± 0.54	75.45 ± 0.56	81.59 ± 0.82	72.37 ± 1.19	79.88 ± 1.06
HiDe-Prompt [45]	NeurIPS23	76.29 ± 0.10	78.77 ± 0.11	76.74 ± 0.18	78.76 ± 0.11	76.46 ± 0.06	78.76 ± 0.11
EvoPrompt [46]	AAAI24	77.16 ± 0.18	82.22 ± 0.54	76.83 ± 0.08	82.09 ± 0.68	74.41 ± 0.23	80.96 ± 1.42
InfLoRA [8]	CVPR24	79.82 ± 0.27	84.07 ± 0.48	78.10 ± 0.43	83.47 ± 1.23	73.81 ± 0.47	81.02 ± 0.56
VQ-Prompt [47]	NeurIPS24	79.23 ± 0.29	82.96 ± 0.50	78.71 ± 0.22	83.24 ± 0.68	78.10 ± 0.22	82.70 ± 1.16
VPT-NSP ² [9]	NeurIPS24	79.71 ± 0.22	84.54 ± 0.68	79.35 ± 0.19	84.92 ± 0.41	76.72 ± 0.44	82.91 ± 0.60
S-LoRA [48]	ICLR25	79.15 ± 0.20	83.01 ± 0.42	77.34 ± 0.35	82.04 ± 0.24	75.26 ± 0.37	80.22 ± 0.72
SplitLoRA	This work	81.92 ± 0.29	85.83 ± 0.55	81.00 ± 0.17	85.84 ± 0.62	78.82 ± 0.28	84.57 ± 0.44

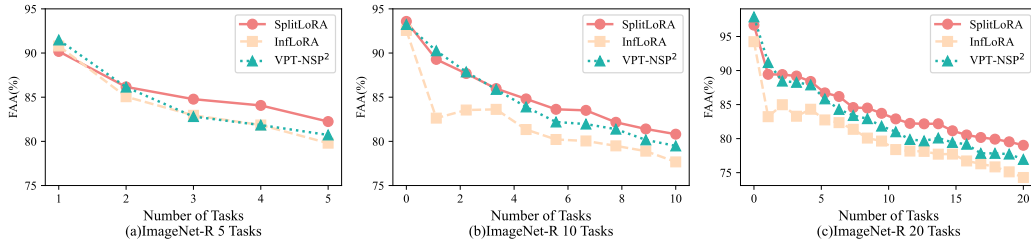


Figure 2: Variation of the performance of different methods during the learning of ImageNet-R.

5 Experiment

5.1 Experimental Settings

Datasets. We conducted experiments on three standard datasets: ImageNet-R [49], CIFAR-100 [50], and DomainNet [51]. ImageNet-R is a variant of ImageNet with 200 classes. CIFAR-100 consists of 100 classes, each containing 600 images. DomainNet contains images from diverse domains, posing a challenge for cross-domain generalization. Following [7, 5, 8], we divided ImageNet-R into 5, 10, and 20 tasks, with each task comprising 40, 20, and 10 classes, respectively. CIFAR-100 was split into 10 tasks, each containing 10 classes, while DomainNet was uniformly partitioned into 5 tasks.

Baselines and Evaluation Metrics. We compare our method with several state-of-the-art continual learning approaches, including L2P++ [5], Deep L2P++ [5], DualPrompt [44], CODA-P [6], HiDe-Prompt [45], EvoPrompt [46], VQ-Prompt [47], VPT-NSP², and InfLoRA [8]. The “Upper bound” represents the performance achieved by jointly training on all classes in one go. Results are averaged over three runs with different random seeds. Following [47], we report Final Average Accuracy (FAA) and Cumulative Average Accuracy (CAA). For details, please refer to the appendix A.3.

Implementation Details. We follow prior works [5, 44, 6, 45, 53, 46] and adopt ViT-Base [35] pre-trained on ImageNet-21K [54] as the backbone. The LoRA rank is set to 10, and the embedding dimension is $D = 768$, matching the feature dimension of ViT-Base[35]. Following [8], we insert SplitLoRA modules into the key and value projections in multi-head attention. Our method is optimized using AdamW [55] with an initial learning rate of $1e-3$ for LoRA and $1e-2$ for the classification head. We use a batch size of 256 across all datasets, and each task is trained for 10 epochs. All experiments are conducted on a single NVIDIA GeForce L40S GPU. All results are reported as mean ± standard deviation over three random seeds.

Table 2: We present FAA (%) and CAA(%) on CIFAR100: 10 tasks and DomainNet: 5 tasks. We report results over 3 trials. All backbone networks are pre-trained on ImageNet-21K.

Method	Pub.	CIFAR100		DomainNet	
		FAA (\uparrow)	CAA (\uparrow)	FAA (\uparrow)	CAA (\uparrow)
Upper-bound	–	91.92 \pm 0.05	–	90.12 \pm 0.13	–
DualPrompt [44]	ECCV22	84.42 \pm 0.30	90.06 \pm 0.07	72.14 \pm 0.05	77.71 \pm 0.06
CODA-Prompt [6]	CVPR23	86.62 \pm 0.11	91.08 \pm 0.28	73.23 \pm 0.13	78.72 \pm 0.07
LAE [7]	ICCV23	84.15 \pm 0.16	89.84 \pm 0.03	66.85 \pm 0.40	75.01 \pm 0.17
C-LoRA [52]	TMLR24	82.97 \pm 0.47	88.81 \pm 0.34	69.34 \pm 0.16	75.25 \pm 0.11
InfLoRA [8]	CVPR24	87.06 \pm 0.25	91.59 \pm 1.43	78.26 \pm 0.50	78.82 \pm 0.34
VPT-NSP ² [9]	NeurIPS24	88.04 \pm 0.11	92.25 \pm 0.80	83.83 \pm 0.19	88.63 \pm 0.10
SplitLoRA	This work	90.33 \pm 0.73	93.70 \pm 0.32	84.31 \pm 0.23	88.99 \pm 0.57

Table 3: We present FAA (%) and CAA(%) on ImageNet-R: 10-tasks. Backbones are with different self-supervised pre-training paradigms: iBOT-1K and DINO-1K.

Method	Pub.	iBOT-1K		DINO-1K	
		FAA \uparrow	CAA \uparrow	FAA \uparrow	CAA \uparrow
Upper-bound	–	84.09 \pm 0.21	–	81.98 \pm 0.07	–
DualPrompt [44]	ECCV22	61.51 \pm 1.05	67.11 \pm 0.08	58.57 \pm 0.45	64.89 \pm 0.15
CODA-Prompt [6]	CVPR23	66.56 \pm 0.68	73.14 \pm 0.57	63.15 \pm 0.39	69.73 \pm 0.25
HiDe-Prompt [45]	NeurIPS23	71.33 \pm 0.21	73.62 \pm 0.13	68.11 \pm 0.18	71.70 \pm 0.01
InfLoRA [8]	CVPR24	71.84 \pm 0.09	78.29 \pm 0.09	68.31 \pm 0.28	76.15 \pm 0.05
VPT-NSP ² [9]	NeurIPS24	73.85 \pm 0.23	80.34 \pm 0.60	69.45 \pm 0.74	76.38 \pm 0.50
VQ-Prompt [47]	NeurIPS24	71.68 \pm 0.72	76.66 \pm 0.40	68.42 \pm 0.28	74.43 \pm 0.58
SplitLoRA	This work	74.58 \pm 1.05	81.45 \pm 1.72	70.49 \pm 0.31	78.15 \pm 1.13

5.2 Experimental Results

Results on ImageNet-R, CIFAR100 and Domainet. Table 1 presents the results of different methods evaluated on ImageNet-R with varying numbers of tasks. It highlights how our proposed method, SplitLoRA, achieves consistently higher accuracy compared to existing continual learning methods across different task setups. Additionally, Table 2 shows the results of these methods on CIFAR100 and DomainNet datasets. Across both tables, SplitLoRA outperforms other methods in FAA and CAA. Figure 2 shows the accuracy trends of various CL methods on ImageNet-R. Our method achieves the highest accuracy at the end and outperforms others throughout the learning curve.

Variant Pre-trained Models. Table 3 provides a summary of experimental results on the 10-task ImageNet-R dataset using different self-supervised pre-training paradigms. Specifically, we evaluate our method with iBOT-1K [56] and DINO-1K [57] pre-training frameworks. These results clearly demonstrate that SplitLoRA consistently outperforms state-of-the-art continual learning methods, irrespective of the pre-training paradigm used. This robustness underscores the generalizability and effectiveness of SplitLoRA in leveraging self-supervised pre-training for continual learning tasks.

Table 5: Impact of different \mathbf{A}_t initialization strategies on ImageNet-R.

Init of \mathbf{A}_t	5 tasks	10 tasks	20 tasks
Random	76.57	76.13	72.30
InfLoRA	78.92	78.10	73.81
SplitLoRA	81.92	81.00	78.82

Table 6: Efficiency of LoRA variants on ImageNet-R (10 tasks).

Method	Extra Fwd	Mem	Time
LoRA	None	22.80 GB	1h 37m
InfLoRA	2/task	23.06 GB	1h 48m
SplitLoRA	1/task	23.03 GB	1h 43m

Initialization strategies of \mathbf{A}_t . Table 5 compares different initialization strategies for \mathbf{A}_t . SplitLoRA achieves consistently better performance across task splits, demonstrating the effectiveness of using projected minor subspace over random or InfLoRA.

Memory and Time Cost. Table 6 shows that SplitLoRA achieves a favorable trade-off between performance and efficiency. It introduces only 1 extra forward pass per task while maintaining similar memory and runtime overheads compared to InfLoRA.

Table 4: Evaluation of model performance under different values of α on ImageNet-R. A higher α may improve plasticity but could impact stability.

Method	5-task		10-task		20-task	
	FAA (\uparrow)	CAA (\uparrow)	FAA (\uparrow)	CAA (\uparrow)	FAA (\uparrow)	CAA (\uparrow)
InfLoRA	79.82	84.07	78.10	83.47	73.81	81.02
SplitLoRA($\alpha = 30$)	82.15	85.60	81.03	85.56	78.73	84.06
SplitLoRA($\alpha = 20$)	81.92	85.83	81.00	85.84	78.82	84.57
SplitLoRA($\alpha = 10$)	82.35	85.82	81.03	85.67	77.89	83.27
SplitLoRA($\alpha = 5$)	82.52	85.89	81.38	85.89	78.15	84.19
SplitLoRA($\alpha = 1$)	82.40	85.86	80.89	85.22	78.59	84.20

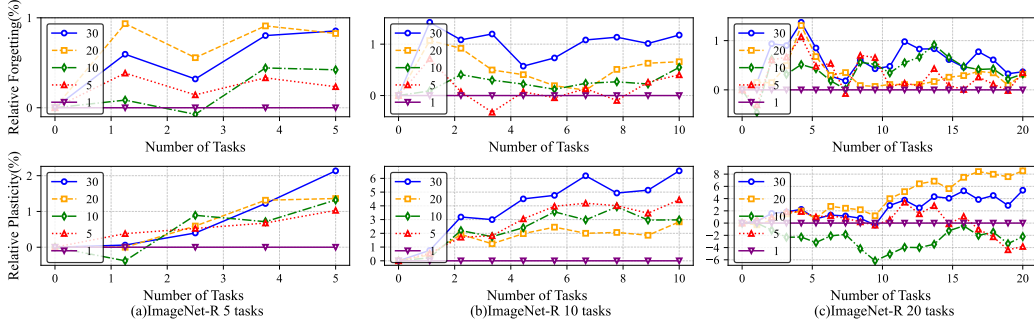


Figure 3: The impact of α on the stability and plasticity of the model in continual learning. As α increases, stability decreases (higher forgetting) while plasticity improves, illustrating the trade-off between retaining past knowledge and adapting to new tasks.

5.3 Hyperparameter Analysis and Discussion

We study the effect of the hyperparameter α on continual learning performance. As shown in Table 4, changing α has limited impact on final accuracy, and all settings consistently outperform InfLoRA. Model stability is measured by *forgetting*, defined as the average gap between each task’s best historical accuracy and its current accuracy. Lower forgetting indicates better knowledge retention. For clarity, we define *relative forgetting* as the difference from the setting where $\alpha = 1$. Plasticity is evaluated by the model’s accuracy on the current task. Similarly, *relative plasticity* is defined as the difference from the plasticity when $\alpha = 1$.

Figure 3 presents results on 5-, 10-, and 20-task splits of ImageNet-R. As α increases, forgetting grows (lower stability) while plasticity improves. These results show that α effectively controls the trade-off between retaining past knowledge and adapting to new tasks, while consistently maintaining better performance than InfLoRA across all settings.

6 Conclusion

In this paper, we investigate the problem of continual learning based on pre-trained ViT models and propose the SplitLoRA method. Specifically, we partition the gradient space of previous tasks into a major subspace and a minor subspace and theoretically model the impact of the minor subspace size on stability and plasticity. After simplifying the optimization problem, we compute the optimal minor subspace size during the continual learning process. Finally, we employ random projection to map the minor subspace onto the low-dimensional matrix of LoRA. Experiments on multiple benchmark datasets demonstrate that our method effectively achieves state-of-the-art performance.

Limitation. In estimating the optimal subspace size, we assume that the ratio between the gradients of the new and previous tasks remains constant. While experimental results suggest that this assumption is robust and effective in practice, it may not be the most principled or optimal solution.

References

- [1] German I Parisi, Ronald Kemker, Jose L Part, Christopher Kanan, and Stefan Wermter. Continual lifelong learning with neural networks: A review. *Neural Networks*, 113:54–71, 2019.
- [2] Edward J Hu, Phillip Wallis, Zeyuan Allen-Zhu, Yuanzhi Li, Shean Wang, Lu Wang, Weizhu Chen, et al. Lora: Low-rank adaptation of large language models. In *International Conference on Learning Representations*, 2022.
- [3] Neil Houlsby, Andrei Giurgiu, Stanislaw Jastrzebski, Bruna Morrone, Quentin De Laroussilhe, Andrea Gesmundo, Mona Attariyan, and Sylvain Gelly. Parameter-efficient transfer learning for nlp. In *Proceedings of the International Conference on Machine Learning*, pages 2790–2799, 2019.
- [4] Menglin Jia, Luming Tang, Bor-Chun Chen, Claire Cardie, Serge J. Belongie, Bharath Hariharan, and Ser-Nam Lim. Visual prompt tuning. In *Proceedings of the European Conference on Computer Vision*, pages 709–727, 2022.
- [5] Zifeng Wang, Zizhao Zhang, Chen-Yu Lee, Han Zhang, Ruoxi Sun, Xiaoqi Ren, Guolong Su, Vincent Perot, Jennifer Dy, and Tomas Pfister. Learning to prompt for continual learning. In *Proceedings of the IEEE/CVF Conference on Computer Vision and Pattern Recognition*, pages 139–149, 2022.
- [6] James Seale Smith, Leonid Karlinsky, Vyshnavi Gutta, Paola Cascante-Bonilla, Donghyun Kim, Assaf Arbelle, Rameswar Panda, Rogerio Feris, and Zsolt Kira. Coda-prompt: Continual decomposed attention-based prompting for rehearsal-free continual learning. In *Proceedings of the IEEE/CVF Conference on Computer Vision and Pattern Recognition*, pages 11909–11919, 2023.
- [7] Qiankun Gao, Chen Zhao, Yifan Sun, Teng Xi, Gang Zhang, Bernard Ghanem, and Jian Zhang. A unified continual learning framework with general parameter-efficient tuning. In *Proceedings of the IEEE/CVF International Conference on Computer Vision*, pages 11449–11459, 2023.
- [8] Yan-Shuo Liang and Wu-Jun Li. Inflora: Interference-free low-rank adaptation for continual learning. In *Proceedings of the IEEE/CVF Conference on Computer Vision and Pattern Recognition*, pages 23638–23647, 2024.
- [9] Yue Lu, Shizhou Zhang, De Cheng, Yinghui Xing, Nannan Wang, Peng Wang, and Yan-ning Zhang. Visual prompt tuning in null space for continual learning. *arXiv preprint arXiv:2406.05658*, 2024.
- [10] Shuyang Jiang, Yusheng Liao, Ya Zhang, Yanfeng Wang, and Yu Wang. Taia: Large language models are out-of-distribution data learners. *arXiv preprint arXiv:2405.20192*, 2024.
- [11] Damai Dai, Li Dong, Yaru Hao, Zhifang Sui, Baobao Chang, and Furu Wei. Knowledge neurons in pretrained transformers. *arXiv preprint arXiv:2104.08696*, 2021.
- [12] Mor Geva, Roei Schuster, Jonathan Berant, and Omer Levy. Transformer feed-forward layers are key-value memories. *arXiv preprint arXiv:2012.14913*, 2020.
- [13] Brian Lester, Rami Al-Rfou, and Noah Constant. The power of scale for parameter-efficient prompt tuning. In Marie-Francine Moens, Xuanjing Huang, Lucia Specia, and Scott Wen-tau Yih, editors, *Proceedings of the Conference on Empirical Methods in Natural Language Processing*, pages 3045–3059, 2021.
- [14] Xiang Lisa Li and Percy Liang. Prefix-tuning: Optimizing continuous prompts for generation. In *Proceedings of the Annual Meeting of the Association for Computational Linguistics*, pages 4582–4597, 2021.
- [15] Elad Ben Zaken, Yoav Goldberg, and Shauli Ravfogel. Bitfit: Simple parameter-efficient fine-tuning for transformer-based masked language-models. In *Proceedings of the Annual Meeting of the Association for Computational Linguistics (Short Papers)*, pages 1–9, 2022.

- [16] Chin-Lun Fu, Zih-Ching Chen, Yun-Ru Lee, and Hung-Yi Lee. Adapterbias: Parameter-efficient token-dependent representation shift for adapters in nlp tasks. In *Findings of the Association for Computational Linguistics*, pages 2608–2621, 2022.
- [17] Rabeeh Karimi Mahabadi, James Henderson, and Sebastian Ruder. Compacter: Efficient low-rank hypercomplex adapter layers. In *Advances in Neural Information Processing Systems*, pages 1022–1035, 2021.
- [18] Shoufa Chen, Chongjian Ge, Zhan Tong, Jiangliu Wang, Yibing Song, Jue Wang, and Ping Luo. Adaptformer: Adapting vision transformers for scalable visual recognition. *Advances in Neural Information Processing Systems*, pages 16664–16678, 2022.
- [19] Friedemann Zenke, Ben Poole, and Surya Ganguli. Continual learning through synaptic intelligence. In *ICML*, pages 3987–3995, 2017.
- [20] Sangwon Jung, Hongjoon Ahn, Sungmin Cha, and Taesup Moon. Continual learning with node-importance based adaptive group sparse regularization. *Advances in Neural Information Processing Systems*, pages 3647–3658, 2020.
- [21] Rahaf Aljundi, Francesca Babiloni, Mohamed Elhoseiny, Marcus Rohrbach, and Tinne Tuytelaars. Memory aware synapses: Learning what (not) to forget. In *ECCV*, pages 139–154, 2018.
- [22] James Kirkpatrick, Razvan Pascanu, Neil Rabinowitz, Joel Veness, Guillaume Desjardins, Andrei A Rusu, Kieran Milan, John Quan, Tiago Ramalho, Agnieszka Grabska-Barwinska, et al. Overcoming catastrophic forgetting in neural networks. *PNAS*, 114(13):3521–3526, 2017.
- [23] Rahaf Aljundi, Eugene Belilovsky, Tinne Tuytelaars, Laurent Charlin, Massimo Caccia, Min Lin, and Lucas Page-Caccia. Online continual learning with maximal interfered retrieval. In *Advances in Neural Information Processing Systems*, pages 11849–11860, 2019.
- [24] Rahaf Aljundi, Min Lin, Baptiste Goujaud, and Yoshua Bengio. Gradient based sample selection for online continual learning. In *Advances in Neural Information Processing Systems*, pages 11816–11825, 2019.
- [25] Qing Sun, Fan Lyu, Fanhua Shang, Wei Feng, and Liang Wan. Exploring example influence in continual learning. *Advances in Neural Information Processing Systems*, pages 27075–27086, 2022.
- [26] Yan-Shuo Liang and Wu-Jun Li. Loss decoupling for task-agnostic continual learning. In Alice Oh, Tristan Naumann, Amir Globerson, Kate Saenko, Moritz Hardt, and Sergey Levine, editors, *Advances in Neural Information Processing Systems*, 2023.
- [27] Andrei A Rusu, Neil C Rabinowitz, Guillaume Desjardins, Hubert Soyer, James Kirkpatrick, Koray Kavukcuoglu, Razvan Pascanu, and Raia Hadsell. Progressive neural networks. *arXiv preprint arXiv:1606.04671*, 2016.
- [28] Steven C. Y. Hung, Cheng-Hao Tu, Cheng-En Wu, Chien-Hung Chen, Yi-Ming Chan, and Chu-Song Chen. Compacting, picking and growing for unforgetting continual learning. In *Advances in Neural Information Processing Systems*, pages 13647–13657, 2019.
- [29] Xilai Li, Yingbo Zhou, Tianfu Wu, Richard Socher, and Caiming Xiong. Learn to grow: A continual structure learning framework for overcoming catastrophic forgetting. In *Proceedings of the International Conference on Machine Learning*, pages 3925–3934, 2019.
- [30] Guanxiong Zeng, Yang Chen, Bo Cui, and Shan Yu. Continual learning of context-dependent processing in neural networks. *Nature Machine Intelligence*, 1(8):364–372, 2019.
- [31] Mehrdad Farajtabar, Navid Azizan, Alex Mott, and Ang Li. Orthogonal gradient descent for continual learning. In *AISTATS*, pages 3762–3773, 2020.
- [32] Gobinda Saha, Isha Garg, and Kaushik Roy. Gradient projection memory for continual learning. In *ICLR*, 2021.

- [33] Sen Lin, Li Yang, Deliang Fan, and Junshan Zhang. Trgp: Trust region gradient projection for continual learning. *arXiv preprint arXiv:2202.02931*, 2022.
- [34] Kaiming He, Xinlei Chen, Saining Xie, Yanghao Li, Piotr Dollár, and Ross Girshick. Masked autoencoders are scalable vision learners. In *Proceedings of the IEEE/CVF Conference on Computer Vision and Pattern Recognition*, pages 16000–16009, 2022.
- [35] Alexey Dosovitskiy, Lucas Beyer, Alexander Kolesnikov, Dirk Weissenborn, Xiaohua Zhai, Thomas Unterthiner, Mostafa Dehghani, Matthias Minderer, Georg Heigold, Sylvain Gelly, et al. An image is worth 16x16 words: Transformers for image recognition at scale. In *International Conference on Learning Representations*, 2021.
- [36] Jacob Devlin, Ming-Wei Chang, Kenton Lee, and Kristina Toutanova. BERT: pre-training of deep bidirectional transformers for language understanding. In *Proceedings of the Conference of the North American Chapter of the Association for Computational Linguistics*, pages 4171–4186, 2019.
- [37] Matteo Boschini, Lorenzo Bonicelli, Angelo Porrello, Giovanni Bellitto, Matteo Pennisi, Simone Palazzo, Concetto Spampinato, and Simone Calderara. Transfer without forgetting. In *Proceedings of the European Conference on Computer Vision*, pages 692–709, 2022.
- [38] Zangwei Zheng, Mingyuan Ma, Kai Wang, Ziheng Qin, Xiangyu Yue, and Yang You. Preventing zero-shot transfer degradation in continual learning of vision-language models. In *Proceedings of the IEEE/CVF International Conference on Computer Vision*, pages 19068–19079, 2023.
- [39] Muhammad Gul Zain Ali Khan, Muhammad Ferjad Naeem, Luc Van Gool, Didier Stricker, Federico Tombari, and Muhammad Zeshan Afzal. Introducing language guidance in prompt-based continual learning. In *Proceedings of the IEEE/CVF International Conference on Computer Vision*, pages 11463–11473, 2023.
- [40] Hao Yu, Xin Yang, Xin Gao, Yan Kang, Hao Wang, Junbo Zhang, and Tianrui Li. Personalized federated continual learning via multi-granularity prompt. In *Proceedings of the 30th ACM SIGKDD Conference on Knowledge Discovery and Data Mining*, pages 4023–4034, 2024.
- [41] Xiao Wang, Tianze Chen, Qiming Ge, Han Xia, Rong Bao, Rui Zheng, Qi Zhang, Tao Gui, and Xuanjing Huang. Orthogonal subspace learning for language model continual learning. *arXiv preprint arXiv:2310.14152*, 2023.
- [42] Xisen Jin, Arka Sadhu, Junyi Du, and Xiang Ren. Gradient-based editing of memory examples for online task-free continual learning. *NeurIPS*, 34:29193–29205, 2021.
- [43] Longteng Zhang, Lin Zhang, Shaohuai Shi, Xiaowen Chu, and Bo Li. Lora-fa: Memory-efficient low-rank adaptation for large language models fine-tuning. *arXiv preprint arXiv:2308.03303*, 2023.
- [44] Zifeng Wang, Zizhao Zhang, Sayna Ebrahimi, Ruoxi Sun, Han Zhang, Chen-Yu Lee, Xiaoqi Ren, Guolong Su, Vincent Perot, Jennifer Dy, et al. Dualprompt: Complementary prompting for rehearsal-free continual learning. In *ECCV*, pages 631–648, 2022.
- [45] Liyuan Wang, Jingyi Xie, Xingxing Zhang, Mingyi Huang, Hang Su, and Jun Zhu. Hierarchical decomposition of prompt-based continual learning: Rethinking obscured sub-optimality. *arXiv preprint arXiv:2310.07234*, 2023.
- [46] Muhammad Rifki Kurniawan, Xiang Song, Zhiheng Ma, Yuhang He, Yihong Gong, Yang Qi, and Xing Wei. Evolving parameterized prompt memory for continual learning. In *AAAI*, volume 38, pages 13301–13309, 2024.
- [47] Li Jiao, Qiuxia Lai, Yu Li, and Qiang Xu. Vector quantization prompting for continual learning. *arXiv preprint arXiv:2410.20444*, 2024.
- [48] Anonymous. S-lora: Scalable low-rank adaptation for class incremental learning. *Under review at International Conference on Learning Representations (ICLR)*, 2025.

- [49] Dan Hendrycks, Steven Basart, Norman Mu, Saurav Kadavath, Frank Wang, Evan Dorundo, Rahul Desai, Tyler Zhu, Samyak Parajuli, Mike Guo, et al. The many faces of robustness: A critical analysis of out-of-distribution generalization. In *Proceedings of the IEEE/CVF International Conference on Computer Vision*, pages 8340–8349, 2021.
- [50] A Krizhevsky. Learning multiple layers of features from tiny images. *Master’s thesis, University of Tront*, 2009.
- [51] Xingchao Peng, Qinxun Bai, Xide Xia, Zijun Huang, Kate Saenko, and Bo Wang. Moment matching for multi-source domain adaptation. In *Proceedings of the IEEE/CVF International Conference on Computer Vision*, pages 1406–1415, 2019.
- [52] James Seale Smith, Yen-Chang Hsu, Lingyu Zhang, Ting Hua, Zsolt Kira, Yilin Shen, and Hongxia Jin. Continual diffusion: Continual customization of text-to-image diffusion with c-lora. *archiveEprint: 2304.06027*, 2024.
- [53] Gengwei Zhang, Liyuan Wang, Guoliang Kang, Ling Chen, and Yunchao Wei. Slca: Slow learner with classifier alignment for continual learning on a pre-trained model. In *ICCV*, 2023.
- [54] Tal Ridnik, Emanuel Ben-Baruch, Asaf Noy, and Lihi Zelnik-Manor. Imagenet-21k pretraining for the masses. In *NeurIPS*, 2021.
- [55] Ilya Loshchilov and Frank Hutter. Decoupled weight decay regularization. In *ICLR*, 2018.
- [56] Jinghao Zhou, Chen Wei, Huiyu Wang, Wei Shen, Cihang Xie, Alan Yuille, and Tao Kong. Image bert pre-training with online tokenizer. In *ICLR*, 2022.
- [57] Mathilde Caron, Hugo Touvron, Ishan Misra, Hervé Jégou, Julien Mairal, Piotr Bojanowski, and Armand Joulin. Emerging properties in self-supervised vision transformers. In *Proceedings of the IEEE/CVF International Conference on Computer Vision*, pages 9650–9660, 2021.
- [58] Da-Wei Zhou, Hai-Long Sun, Jingyi Ning, Han-Jia Ye, and De-Chuan Zhan. Continual learning with pre-trained models: A survey. *arXiv preprint arXiv:2401.16386*, 2024.

A Appendix

A.1 Proof of Proposition 4.1

Before proving Proposition 4.1, we first establish a supporting lemma.

Lemma A.1 (Gradient Preservation under Orthogonal Updates). *Let $L_j : \mathbb{R}^d \rightarrow \mathbb{R}$ be a twice-differentiable loss function corresponding to task j , and let W_j be the model parameters after completing task j . Suppose at step $t > j$, the update direction \tilde{g}_t for task t satisfies $\langle \nabla L_j(W_j), \tilde{g}_t \rangle = 0$. The updated parameter is given by: $W_t = W_j - \eta \tilde{g}_t$. Further assume that the second-order term $\eta H_j \tilde{g}_t$ in the Taylor expansion of ∇L_j can be ignored. Then, the gradient of task j remains unchanged:*

$$\nabla L_j(W_t) = \nabla L_j(W_j).$$

Proof. Since L_j is twice-differentiable, we apply the first-order Taylor expansion of the gradient at point W_j in the direction of \tilde{g}_t :

$$\nabla L_j(W_t) = \nabla L_j(W_j - \eta \tilde{g}_t) = \nabla L_j(W_j) - \eta H_j \tilde{g}_t + o(\eta).$$

Now, under the assumption that $\eta H_j \tilde{g}_t$ is negligible (i.e., small learning rate and low curvature), we ignore the second-order term:

$$\nabla L_j(W_t) = \nabla L_j(W_j).$$

□

Based on the Lemma A.1, we denote $\nabla L_i(W_j)$ as \mathbf{G}_i . Next, we provide the proof of Proposition 4.1.

Proposition 4.1. Assume the loss $\mathcal{L}_i(\mathbf{W})$ is L -smooth for all $i \in \{1, \dots, t\}$. Let the model update be $\mathbf{W}_t = \mathbf{W}_{t-1} + \Delta \mathbf{W}_t$. Then:

$$\sum_{i=1}^t (\mathcal{L}_i(\mathbf{W}_t) - \mathcal{L}_i(\mathbf{W}_{t-1})) \leq -(t-1) \langle \Delta \mathbf{W}_t, \mathbf{G}_t^{\text{old}} \rangle - \langle \Delta \mathbf{W}_t, \mathbf{G}_t \rangle + \frac{(t-1)L}{2} \|\Delta \mathbf{W}_t\|_F^2.$$

Proof. By L -smoothness of each \mathcal{L}_i , we have:

$$\mathcal{L}_i(\mathbf{W}_t) \leq \mathcal{L}_i(\mathbf{W}_{t-1}) + \langle \nabla \mathcal{L}_i(\mathbf{W}_{t-1}), \Delta \mathbf{W}_t \rangle + \frac{L}{2} \|\Delta \mathbf{W}_t\|_F^2.$$

Summing over $i = 1$ to t :

$$\sum_{i=1}^t \mathcal{L}_i(\mathbf{W}_t) - \sum_{i=1}^t \mathcal{L}_i(\mathbf{W}_{t-1}) \leq \sum_{i=1}^t \langle \nabla \mathcal{L}_i(\mathbf{W}_{t-1}), \Delta \mathbf{W}_t \rangle + \frac{tL}{2} \|\Delta \mathbf{W}_t\|_F^2.$$

Let $\mathbf{G}_t^{\text{old}} = \frac{1}{t-1} \sum_{i=1}^{t-1} \nabla \mathcal{L}_i(\mathbf{W}_{t-1})$, then:

$$\sum_{i=1}^{t-1} \langle \nabla \mathcal{L}_i(\mathbf{W}_{t-1}), \Delta \mathbf{W}_t \rangle = (t-1) \langle \mathbf{G}_t^{\text{old}}, \Delta \mathbf{W}_t \rangle.$$

Substituting back gives:

$$\sum_{i=1}^t (\mathcal{L}_i(\mathbf{W}_t) - \mathcal{L}_i(\mathbf{W}_{t-1})) \leq -(t-1) \langle \Delta \mathbf{W}_t, \mathbf{G}_t^{\text{old}} \rangle - \langle \Delta \mathbf{W}_t, \mathbf{G}_t \rangle + \frac{(t-1)L}{2} \|\Delta \mathbf{W}_t\|_F^2.$$

□

A.2 Proof of Theorem 4.2

Let \mathbf{W}_{t-1} denote the weight matrix of a linear layer in the model, updated as $\mathbf{W}_t = \mathbf{W}_{t-1} + \Delta \hat{\mathbf{W}}_t = \mathbf{W}_{t-1} + \mathbf{U}_t^k \mathbf{U}_t^{k\top} \Delta \mathbf{W}_t$. Since the update direction of the new task is unknown, we assume that it is uniformly distributed across all directions. that is to say, $\Delta \mathbf{W}_t$ has the same expected projection value across different feature directions of \mathbf{G}_t , we provide the expected values of the stability loss :

$$\mathbb{E}[\mathcal{L}_t^S(\mathbf{W}_t)] = -(t-1)\epsilon_t(k_t) \langle \Delta \mathbf{W}_t, \mathbf{G}_t^{\text{old}} \rangle, \quad (18)$$

and the plasticity loss:

$$\mathbb{E}[\mathcal{L}_t^P(\mathbf{W}_t)] = -\frac{k_t}{d} \langle \Delta \mathbf{W}_t, \mathbf{G}_t \rangle. \quad (19)$$

Proof. Stability Loss:

By definition, the projected update is:

$$\Delta \hat{\mathbf{W}}_t = \mathbf{U}_t^k \mathbf{U}_t^{k\top} \Delta \mathbf{W}_t.$$

Thus, the expected stability loss is:

$$\begin{aligned} \mathbb{E}[\mathcal{L}_t^S] &= -(t-1)\mathbb{E}[\langle \Delta \hat{\mathbf{W}}_t, \mathbf{G}_t^{\text{old}} \rangle] \\ &= -(t-1)\mathbb{E}[\langle \mathbf{U}_t^k \mathbf{U}_t^{k\top} \Delta \mathbf{W}_t, \mathbf{G}_t^{\text{old}} \rangle] \\ &= -(t-1)\mathbb{E}[\text{Tr}(\Delta \mathbf{W}_t^\top \mathbf{U}_t^k \mathbf{U}_t^{k\top} \mathbf{G}_t^{\text{old}})]. \end{aligned}$$

Let $\mathbf{G}_t^{\text{old}} = \sum_{i=1}^d \sigma_i \mathbf{u}_i \mathbf{v}_i^\top$ be the SVD. Then,

$$\mathbf{U}_t^k \mathbf{U}_t^{k\top} \mathbf{G}_t^{\text{old}} = \sum_{i=d-k_t+1}^d \sigma_i \mathbf{u}_i \mathbf{v}_i^\top.$$

So:

$$\mathbb{E}[\mathcal{L}_t^S] = -(t-1) \sum_{i=d-k_t+1}^d \sigma_i \cdot \mathbb{E}[\langle \Delta \mathbf{W}_t, \mathbf{u}_i \mathbf{v}_i^\top \rangle_F].$$

Under the uniform distribution assumption, all expected projections are equal:

$$\mathbb{E}[\langle \Delta \mathbf{W}_t, \mathbf{u}_i \mathbf{v}_i^\top \rangle_F] = c, \quad \forall i.$$

Then:

$$\mathbb{E}[\mathcal{L}_t^S] = -(t-1) \cdot c \cdot \sum_{i=d-k_t+1}^d \sigma_i.$$

Also,

$$\langle \Delta \mathbf{W}_t, \mathbf{G}_t^{\text{old}} \rangle = \sum_{i=1}^d \sigma_i \cdot \langle \Delta \mathbf{W}_t, \mathbf{u}_i \mathbf{v}_i^\top \rangle_F = c \cdot \sum_{i=1}^d \sigma_i,$$

so:

$$c = \frac{\langle \Delta \mathbf{W}_t, \mathbf{G}_t^{\text{old}} \rangle}{\sum_{i=1}^d \sigma_i}.$$

Thus,

$$\mathbb{E}[\mathcal{L}_t^S] = -(t-1) \cdot \epsilon_t(k_t) \cdot \langle \Delta \mathbf{W}_t, \mathbf{G}_t^{\text{old}} \rangle.$$

—

Plasticity Loss:

The plasticity loss is:

$$\mathbb{E}[\mathcal{L}_t^P] = -\mathbb{E}[\langle \Delta \hat{\mathbf{W}}_t, \mathbf{G}_t \rangle] = -\mathbb{E}[\langle \mathbf{U}_t^k \mathbf{U}_t^{k\top} \Delta \mathbf{W}_t, \mathbf{G}_t \rangle].$$

Let $\alpha_i = \langle \Delta \mathbf{W}_t, \mathbf{u}_i \rangle$, $\beta_i = \langle \mathbf{G}_t, \mathbf{u}_i \rangle$. Then:

$$\mathbb{E}[\mathcal{L}_t^P] = -\mathbb{E} \left[\sum_{i=1}^{k_t} \alpha_i \beta_i \right].$$

Under the uniform assumption, the expected contribution over any direction is $\frac{1}{d}$, hence:

$$\mathbb{E}[\mathcal{L}_t^P] = -\frac{k_t}{d} \cdot \langle \Delta \mathbf{W}_t, \mathbf{G}_t \rangle.$$

□

A.3 Evaluation metrics

To evaluate continual learning performance, we track the average classification accuracy over all classes encountered so far at the end of each task’s training following [47]. We denote by A_{ij} the average accuracy on the i -th task after training the j -th task. Below, we provide formal definitions for two key metrics: FAA and CAA.

(i) Final Average Accuracy (FAA). FAA measures the overall performance after learning all tasks, defined as:

$$\text{FAA} = \frac{1}{T} \sum_{i=1}^T A_{iT}, \quad (20)$$

where T is the total number of tasks and A_{iT} is the accuracy for task i after completing task T . A larger FAA indicates a stronger ability to learn while minimizing forgetting. In some literature, FAA is also referred to as “Last-Acc.”

(ii) Cumulative Average Accuracy (CAA). CAA is the average of the FAA values computed after each task is learned, given by:

$$\text{CAA} = \frac{1}{T} \sum_{j=1}^T \frac{1}{j} \sum_{i=1}^j A_{ij}. \quad (21)$$

It captures the overall performance at every incremental step. This metric is sometimes referred to as “Inc-Acc.”

A.4 The size of minor subspace evolves during training.

We tracked the evolution of the minor subspace size throughout training on ImageNet-R with 20 tasks. As shown in the figure 4, as the number of tasks increases, model stability becomes more critical, leading to a progressively smaller minor subspace. Furthermore, when comparing different layers of ViT, the minor subspace is larger in shallower layers and gradually decreases as the layer depth increases. This suggests that changes in the deep-layer parameters have a greater impact on model stability.

When the value of α varies, the model’s learning space changes significantly; nevertheless, the model is still able to learn tasks effectively in all cases. Here, we introduce a simple experiment to explain it. As Tab. 7 shows, "Only head" means training only the classifier head for each task; "Only head and the first task" means training the first task’s LoRA and the classifiers for all tasks. SplitLoRA is used for comparison. It can be observed that even when only the classifier is trained, the model can still learn effectively, and when subsequent tasks are fine-tuned on the first task’s LoRA, performance improves. The knowledge contained in the pre-trained model and the beneficial knowledge from old tasks help the new task’s learning.

Table 7: Average accuracy of tasks 2–20 under different fine-tuning strategies.

Method	Avg. Acc (Tasks 2–20)
Only head	66.08
Only head and the first task	74.75
SplitLoRA	81.47

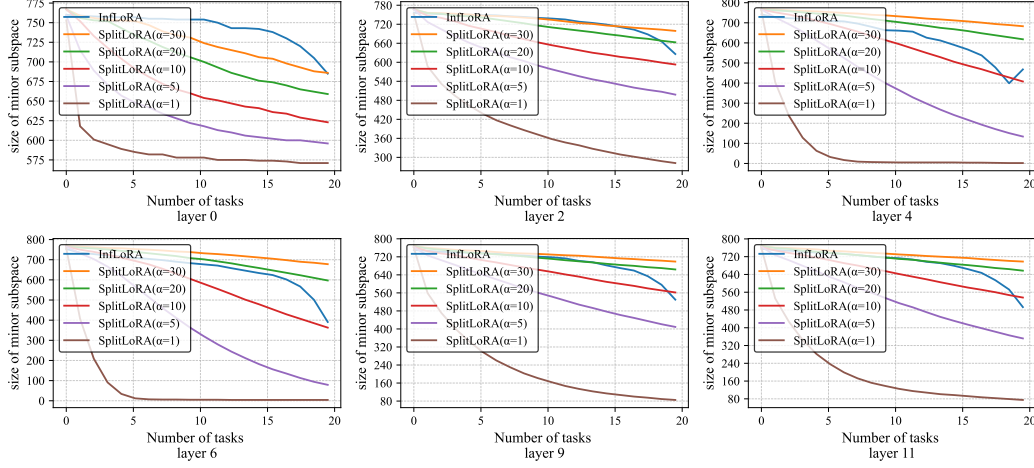


Figure 4: We recorded the evolution of the minor subspace size during training on ImageNet-R with 20 tasks.

A.5 More results on other benchmark.

We further evaluate the performance of SplitLoRA on another benchmark [58]. Tab. 8 compares SplitLoRA with state-of-the-art continual learning methods on seven benchmarks. SplitLoRA achieves the best average performance (79.95%) and consistently ranks top in individual tasks. In particular, it excels on ImageNet-R, Omni, and VTAB, demonstrating strong generalization and knowledge retention. This confirms that SplitLoRA effectively balances stability and plasticity across diverse scenarios.

Table 8: Comparison with state-of-the-art methods on multiple benchmarks. We report CAA and FAA (%) on base and incremental sessions.

Method	CIFAR B0 Inc5	CUB B0 Inc10	IN-R B0 Inc5	IN-A B0 Inc20	Obj B0 Inc10	Omni B0 Inc30	VTAB B0 Inc10	Average
L2P	85.94 / 79.93	67.05 / 56.25	66.53 / 59.22	49.39 / 41.71	63.78 / 52.19	73.36 / 64.69	77.11 / 77.10	65.30
DualPrompt	87.87 / 81.15	77.47 / 66.54	63.31 / 55.22	53.71 / 41.67	59.27 / 49.33	73.92 / 65.52	83.36 / 81.23	67.11
CODA-Prompt	89.11 / 81.96	84.00 / 73.37	64.42 / 55.08	53.54 / 42.73	66.07 / 53.29	77.03 / 68.09	83.90 / 83.02	69.68
DAP	94.54 / 90.62	94.76 / 94.63	80.61 / 74.76	54.39 / 46.32	72.08 / 59.51	86.44 / 80.65	84.65 / 84.64	78.47
DAP w/o BI	68.07 / 58.16	65.27 / 52.05	50.40 / 37.99	34.48 / 21.84	50.47 / 37.55	65.43 / 52.53	79.63 / 79.87	53.83
SimpleCIL	87.57 / 81.26	92.20 / 86.73	62.58 / 54.55	59.77 / 48.91	65.45 / 53.59	79.34 / 73.15	85.99 / 84.38	72.53
ADAM + VPT-D	88.46 / 82.17	91.02 / 84.99	68.79 / 60.48	58.48 / 48.52	67.83 / 54.65	81.05 / 74.47	86.59 / 83.06	73.61
ADAM + SSF	87.78 / 81.98	91.72 / 86.13	68.94 / 60.60	61.30 / 50.03	69.15 / 56.64	80.53 / 74.00	85.66 / 81.92	74.02
ADAM + Adapter	90.65 / 85.15	92.21 / 86.73	72.35 / 64.33	60.47 / 49.37	67.18 / 55.24	80.75 / 74.37	85.95 / 84.35	74.93
RanPAC	93.51 / 89.30	93.13 / 89.40	75.74 / 68.75	64.16 / 52.86	71.67 / 60.08	85.95 / 79.55	92.56 / 91.83	79.17
EASE	91.51 / 85.80	92.23 / 86.81	78.31 / 70.58	65.34 / 55.04	70.84 / 57.86	81.11 / 74.85	93.61 / 93.55	78.39
HiDe-Prompt	91.22 / 89.92	89.75 / 89.46	76.20 / 74.56	61.41 / 49.27	70.13 / 62.84	76.60 / 77.01	91.24 / 92.78	78.02
ESN	87.15 / 80.37	65.69 / 63.10	60.69 / 55.13	44.06 / 31.07	63.73 / 52.55	75.32 / 66.57	81.52 / 62.15	63.50
SplitLoRA	93.11 / 90.84	91.52 / 87.46	81.74 / 74.81	66.11 / 58.22	68.60 / 61.33	82.30 / 76.86	94.39 / 91.95	79.95